

PROPERTIES OF GALAXY DARK MATTER HALOS FROM WEAK LENSING

HENK HOEKSTRA^{1,2,3}, H.K.C. YEE^{2,3}, AND MICHAEL D. GLADDERS^{3,4}*Draft version March 25, 2019*

ABSTRACT

We present the results of a study of weak lensing by galaxies based on 45.5 deg² of R_C band imaging data from the Red-Sequence Cluster Survey (RCS). We define a sample of lenses with $19.5 < R_C < 21$, and a sample of background galaxies with $21.5 < R < 24$. We study the average mass profile around the lenses, using a maximum likelihood analysis. We consider two models for the halo mass profile: a truncated isothermal sphere (TIS) and an NFW profile. We constrain the power law scaling relations between the B -band luminosity and the velocity dispersion (or rotation velocity) and the size of the halo. The inferred velocity dispersion is in excellent agreement with observed luminosity-line-width relations. The TIS model yields a best fit velocity dispersion of $\sigma = 137 \pm 5$ km/s and a truncation radius $s = 185^{+30}_{-28} h^{-1}$ kpc for a galaxy with a fiducial luminosity of $L_B = 10^{10} h^{-2} L_{B\odot}$. Alternatively, the best fit NFW model yields a mass $M_{200} = (8.8 \pm 0.7) \times 10^{11} h^{-1} M_\odot$ and a scale radius $r_s = 16.7^{+3.7}_{-3.0} h^{-1}$ kpc. This value for the scale radius is in excellent agreement with predictions from numerical simulations for a halo of this mass. Having constrained the virial mass and scaling relations, we can convert the observed luminosity function into a mass function, and estimate the matter density of the universe. Based on numerical simulations, we find that only $\sim 37\%$ of the matter is contained within the virial radius of halos. After correction for this effect, we obtain $\Omega_m = 0.30^{+0.13}_{-0.08}$, in excellent agreement with other recent measurements. We also present the first weak lensing detection of the flattening of galaxy dark matter halos. We use a simple model in which the ellipticity of the halo is f times the observed ellipticity of the lens. We find a best fit value of $f = 0.77^{+0.18}_{-0.21}$ (68% confidence), suggesting that the dark matter halos are somewhat rounder than the light distribution. The fact that we detect a significant flattening implies that the halos are aligned with the light distribution. Given the average ellipticity of the lenses, this implies a halo ellipticity of $\langle e_{\text{halo}} \rangle = 0.20^{+0.04}_{-0.05}$ (68% confidence), in fair agreement with results from numerical simulations of CDM. This result provides strong support for the existence of dark matter, as an isotropic lensing signal is excluded with 99.5% confidence.

Subject headings: cosmology: observations – dark matter – gravitational lensing – galaxies: haloes

1. INTRODUCTION

The existence of massive dark matter halos around galaxies is widely accepted, based on different lines of evidence, such as flat rotation curves of spiral galaxies (e.g., Van Albada & Sancisi 1986) and strong lensing systems (e.g., Keeton, Kochanek & Falco 1998). However, relatively little is known about the properties of dark matter halos. Strong lensing only probes the gravitational potential on small (projected) scales, whereas the lack of visible tracers at large radii hamper dynamical methods. To date, only satellite galaxies have provided some information (e.g., Zaritsky & White 1994; McKay et al. 2002)

A promising approach to study the galaxy dark matter halos is weak gravitational lensing. The tidal gravitational field of the dark matter halo introduces small coherent distortions in the images of distant background galaxies. The weak lensing signal can be measured out to large projected distances from the lens, and hence provides a unique probe of the gravitational potential on large scales.

The applications of this approach are numerous: one can infer masses of galaxies and compare the results to their luminosities (e.g., McKay et al. 2001; Wilson et al. 2001), or one can attempt to constrain the halo mass profile (e.g., Brainerd et al. 1996; Hudson et al. 1998; Fischer et al. 2000; Hoekstra et al. 2003). Also, weak lensing can be used to constrain the shapes of halos by measuring the azimuthal variation of the lensing signal. Unfortunately, one can only study ensemble averaged properties, because the weak lensing signal induced by an individual galaxy is too low to be detected.

A successful measurement of the lensing signal requires large samples of both lenses and background galaxies. The first attempt to detect the lensing signal by galaxies was made by Tyson et al. (1984) using photographic plates. It took more than a decade and CCD cameras before the first detections were reported (Brainerd et al. 1996; Griffiths et al. 1996; Dell’Antonio & Tyson 1996; Hudson et al. 1998). These early results limited by the small areas covered by the observations.

The accuracy with which the galaxy-galaxy lensing signal can be measured depends on the area of sky that is observed, and on the availability of redshifts for the lenses (as it allows for a proper scaling of the lensing signal). Photometric redshifts were used by Hudson et al. (1998) to scale the lensing signal of galaxies in the Hubble Deep Field, and by Wilson et al. (2001) who measured the lens-

¹ CITA, University of Toronto, Toronto, Ontario M5S 3H8, Canada² Department of Astronomy, University of Toronto, Toronto, Ontario M5S 3H8, Canada³ Visiting Astronomer, Canada-France-Hawaii Telescope, which is operated by the National Research Council of Canada, Le Centre National de Recherche Scientifique, and the University of Hawaii⁴ Observatories of the Carnegie Institution of Washington, 813 Santa Barbara Street, Pasadena, California 91101

ing signal around early type galaxies as a function of redshift. Furthermore, several lensing studies targeted regions covered by redshift surveys. Smith et al. (2001) used 790 lenses from the Las Campanas Redshift Survey; Hoekstra et al. (2003) used 1125 lenses from the Canadian Network for Observational Cosmology Field Galaxy Redshift Survey (CNOC2). The areas covered by these surveys are relatively small.

The Sloan Digital Sky Survey (SDSS) combines both survey area and redshift information. Its usefulness for galaxy-galaxy lensing was demonstrated clearly by Fischer et al. (2000). More recently, McKay et al. (2001) used the available SDSS redshift information to study the galaxy-galaxy lensing signal as a function of galaxy properties (also see Guzik & Seljak 2002; Seljak 2002).

The data used in this paper currently lacks redshift information for the lenses. However, compared to previous work, the combination of large area and depth of our observations allow us to measure the galaxy lensing signal with great precision. We use 45.5 deg² of R_C -band imaging data from the Red-Sequence Cluster Survey (RCS). These data have been used previously for several weak lensing studies. Hoekstra et al. (2002a; 2002b) placed joint constraints on Ω_m and σ_8 by measuring the lensing signal caused by large scale structure. Related to the subject of this paper is the study of the bias parameters as a function of scale by Hoekstra et al. (2001b) and Hoekstra et al. (2002c). The latter studies made use of the galaxy-mass cross-correlation function measured from the RCS data. Here we use the galaxy-mass cross-correlation function for a different purpose: we effectively deconvolve the cross-correlation function to study the properties of dark matter halos surrounding galaxies at intermediate redshifts.

The structure of the paper is as follows. In §2 we briefly discuss the data and the redshift distributions of the lenses and the sources. The ensemble averaged tangential shear around the lenses (galaxy-mass cross-correlation function) is presented in §3. In §4 we use a maximum likelihood analysis to derive constraints on the extent of dark matter halos. The measurement of the projected shapes of the halos is presented in §5.

2. OBSERVATIONS AND ANALYSIS

We use the R_C -band imaging data from the Red-Sequence Cluster Survey (Yee & Gladders 2001; Gladders & Yee 2003). The complete survey covers 90 deg² in both R_C and z' , spread over 22 widely separated patches of $\sim 2.1 \times 2.3$ degrees. In this paper we use data from the northern half of the survey, which consists of 10 patches, observed with the CFH12k camera on the CFHT. These data cover 45.5 deg² on the sky, but because of masking the effective area is somewhat smaller. In the lensing analysis we use a total of 42 deg². A detailed description of the data reduction and object analysis can be found in Hoekstra et al. (2002a), to which we refer for technical details. Here we present a short description of the various steps in the analysis.

We use single exposures in our analysis, and consequently cosmic rays have not been removed. However, cosmic rays are readily eliminated from the photometric catalogs: small, but very significant objects are likely to be cosmic rays, or artifacts from the CCD. The object finder

gives fair estimates of the object sizes, and we remove all objects smaller than the size of the PSF.

The objects in this cleaned catalog are then analysed, which yield estimates for the size, apparent magnitude, and shape parameters (polarisation and polarisabilities). The objects in this catalog are inspected by eye, in order to remove spurious detections. These objects have to be removed because their shape measurements are affected by cosmetic defects (such as dead columns, bleeding stars, halos, diffraction spikes) or because the objects are likely to be part of a resolved galaxy (e.g., HII regions).

To measure the small, lensing induced distortions in the images of the faint galaxies it is important to accurately correct the shapes for observational effects, such as PSF anisotropy, seeing and camera shear; PSF anisotropy can mimic a cosmic shear signal, and a correction for the seeing is required to relate the measured shapes to the real lensing signal. To do so, we follow the procedure outlined in Hoekstra et al. (1998). We select a sample of moderately bright stars from our observations, and use these to characterize the PSF anisotropy and seeing. We fit a second order polynomial to the shape parameters of the selected stars for each chip of the CFH12k camera. These results are used to correct the shapes of the galaxies for PSF anisotropy and seeing.

The effect of the PSF is not the only observational distortion that has to be corrected. The optics of the camera stretches the images of galaxies (i.e., it introduces a shear) because of the non-linear remapping of the sky onto the CCD. We have used observations of astrometric fields to find the mapping between the sky and the CCD pixel coordinate system, and derived the corresponding camera shear, which is subsequently subtracted from the galaxy ellipticity (see Hoekstra et al. 1998).

The findings presented in Hoekstra et al. (2002a) suggest that the correction for PSF anisotropy has worked well. The absence of a “B”-mode in the measurements of the cosmic shear (Hoekstra et al. 2002b) provides additional evidence that systematics are well under control. Furthermore, cosmic shear studies are much more sensitive to systematics than galaxy-galaxy lensing measurements (e.g., see Hoekstra et al. 2003). In galaxy-galaxy lensing one measures the lensing signal that is perpendicular to the lines connecting many lens-source pairs. These connecting lines are randomly oriented with respect to the PSF anisotropy, and hence suppress any residual systematics.

2.1. Redshift distributions

For the analysis presented here, we select a sample of “lenses” and “sources” on the basis of their apparent R_C magnitude. We define galaxies with $19.5 < R_C < 21$ as lenses, and galaxies with $21.5 < R_C < 24$ as sources which are used to measure the lensing signal. This selection yields a sample of $\sim 1.2 \times 10^5$ lenses and $\sim 1.5 \times 10^6$ sources.

The amplitude of the lensing signal depends on $\langle \beta \rangle$, the average ratio of the angular diameter distances between the lens and the source, D_{ls} , and the distance between the observer and the source D_s . Hence, to interpret the measurements, such as size and mass, one needs to know the redshift distributions of both lenses and sources.

The CNOC2 Field Galaxy Redshift Survey (e.g., Lin et al. 1999; Yee et al. 2000; Carlberg et al. 2000) has measured the redshift distribution of field galaxies down to $R_C = 21.5$, which is ideal, given our limits of $19.5 < R_C < 21$. The derived redshift distribution gives a median redshift $z = 0.35$ for the lens sample. In addition, we use the redshifts and the colors of the galaxies observed in the CNOC2 survey to compute their rest-frame B luminosity.

Compared to studies using SDSS data (McKay et al. 2001) we have the disadvantage that we do not have (spectroscopic) redshifts for the individual lenses. As shown by Hoekstra et al. (2003) this limits the accuracy of the measurements. Nevertheless, the large area covered by the RCS allows us to derive interesting information about the properties of the lenses. In §4 we use different cuts in apparent magnitude to study the properties of dark matter halos using a maximum likelihood analysis. In effect, we use the apparent magnitude as a very crude redshift indicator. Figure 1 shows the mean redshift of the lenses as a function of apparent magnitude, as well as the observed redshift distributions for the different cuts in apparent magnitude. Multi-color data for the northern part of the RCS will be available in the near future, allowing us to select a sample of lenses based on their photometric redshifts.

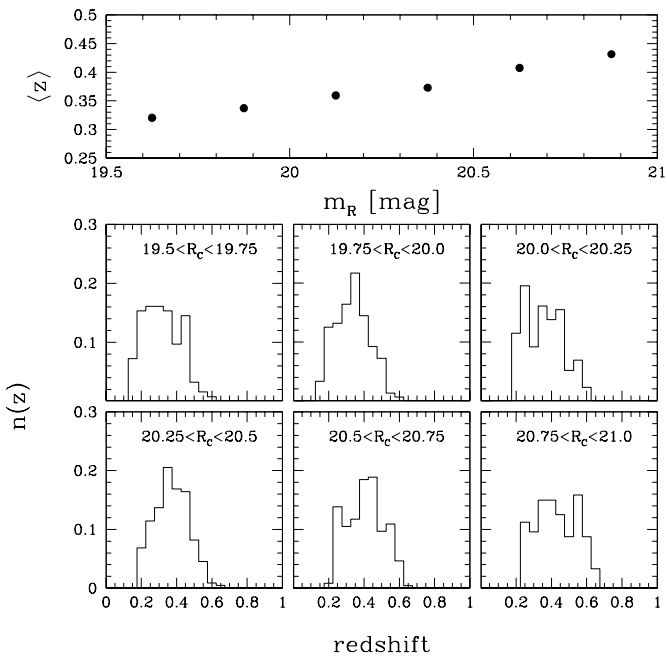


FIG. 1.— Upper panel: mean redshift of the lenses as a function of apparent magnitude. Lower panel: redshift distributions for the different ranges in apparent magnitude, as measured in the CNOC2 redshift survey.

For the source galaxies the situation is more complicated. These galaxies are generally too faint for spectroscopic surveys, although recently Cohen et al. (2000) measured spectroscopic redshifts around the Hubble Deep Field North down to $R_C \sim 24$. Cohen et al. (2000) find that the spectroscopic redshifts agree well with the photometric redshifts derived from multi-color photometry. Because of likely field-to-field variations in the red-

shift distribution, we prefer to use the photometric redshift distributions derived from both Hubble Deep Fields (Fernández-Soto et al. 1999), which yields a median redshift of $z = 0.53$ for the source galaxies. The results in an average value of $\langle \beta \rangle = 0.29 \pm 0.01$ for the full sample of lenses and sources.

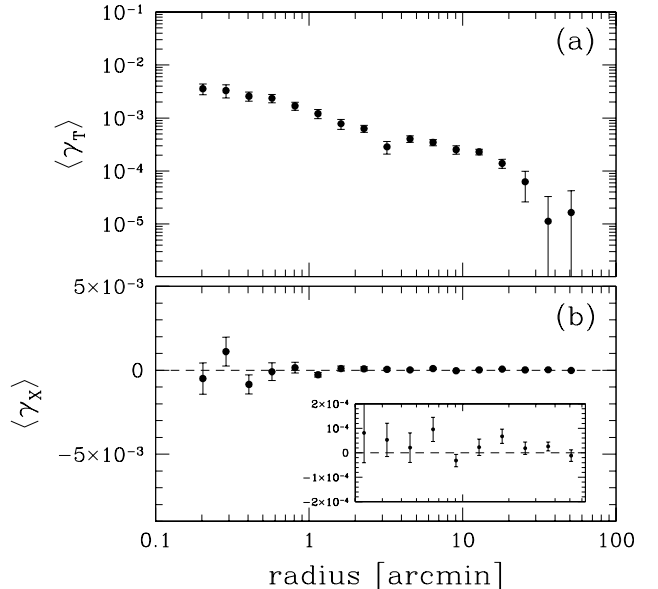


FIG. 2.— (a) The galaxy-mass cross-correlation function as a function of angular scale. The lenses are selected on the basis of their apparent R_C -band magnitude, taking $19.5 < R_C < 21$. The tangential alignment is detected out to a radius of 1 degree. The signal on these large scale no longer reflects the mass of the lens, but the clustering properties of the lenses. (b) The signal when the phase of the shear is increased by $\pi/4$. No signal should be present if the signal detected in panel (a) is caused by gravitational lensing. The results are consistent with no signal. The error bars are so small that we expanded the y-axis by a factor 25 in the inset of panel (b). The complex geometry of the survey on large scales (holes in the survey area because of masking) results in non-vanishing values of γ_X . Despite these complications, the residuals are remarkably small.

3. GALAXY-MASS CROSS-CORRELATION FUNCTION

The galaxy-mass cross-correlation function provides a convenient way to present the measurements. It is obtained from the data by measuring the tangential alignment of the source galaxies with respect to the lens as a function of radius. Its use for studying the halos of galaxies is limited, because the clustering of galaxies complicates a direct interpretation of the signal: on small scales the signal is dominated by the mass distribution of the lens, but on larger scales one measures the superposition of the contributions from many lenses.

The observed galaxy-mass cross-correlation function as a function of angular scale is presented in Figure 2a. A significant signal is detected out to one degree from the lens. If the signal presented in Figure 2a is caused by gravitational lensing, no signal should be present when the phase of the distortion is increased by $\pi/4$ (i.e., when the sources are rotated by 45 degrees). The results of this test, shown in Figure 2b, suggest that residual systematics are negligible.

Before we can interpret the results we need to examine the contribution of foreground galaxies. Some of the source galaxies will be in front of the lenses, and lower the lensing signal independent of radius. This is absorbed in the value of $\langle \beta \rangle$. These galaxies decrease the lensing signal independent of angular scale. Some sources, however, are physically associated with the lenses. These galaxies cluster around the lenses, affecting the lensing signal more on small scales. We need to account for this source of contamination. To do so, we measure a fractional excess of sources around lenses which decreases with radius as $f_{\text{bg}}(r) = 0.93r^{-0.76}$ (r in arcseconds), similar to what was found by Fischer et al. (2000). Under the assumption that the orientations of these galaxies are random (the tidal interaction with the lens has not introduced an additional tangential or radial alignment), the observed lensing signal has to be increased by a factor $f_{\text{bg}}(r)$. This assumption is supported by the findings of Bernstein & Norberg (2002) who examined the tangential alignment of satellite galaxies around galaxies, extracted from the 2dF Galaxy Redshift Survey. The measurements presented in Figures 2 have been corrected for this decrease in signal. We note that the correction for the presence of satellite galaxies is small, and has no significant effect on our results.

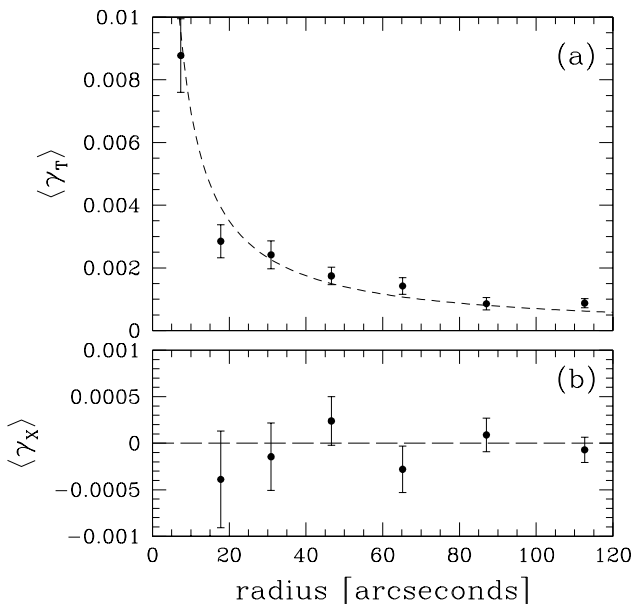


FIG. 3.— (a) Ensemble averaged tangential shear as a function of radius out to 2 arcminutes from the lens. The solid line corresponds to the best fit SIS model to the data at radii smaller than 2 arcminutes. (b) The signal when the phase of the shear is increased by $\pi/4$. Note the different vertical scale between panels a and b.

The signal on small angular scales is dominated by a single lens galaxy, and can be used to obtain an estimate of the mass weighted velocity dispersion of the sample of lenses (although such a mass estimate can still be slightly biased because of the clustering of the lenses). Figure 3a shows the ensemble averaged tangential shear on small scales. The measurements presented in Figure 3b show no evidence for residual systematics.

We fit a singular isothermal sphere (SIS) model to the tangential shear at radii smaller than 2 arcminutes (which

corresponds to $\sim 350h^{-1}$ kpc at the mean redshift of the lenses). The best fit model is indicated by the dashed line in Figure 3a. For the Einstein radius r_E we obtain a value of $\langle r_E \rangle = 0''.140 \pm 0''.009$. If we extend the fit to much larger radii, the inferred value for the Einstein radius increases systematically. With our adopted redshift distributions for the lenses and the sources, the value of r_E corresponds to a value of $\langle \sigma^2 \rangle^{1/2} = 128 \pm 4$ km/s. The corresponding circular velocity can be obtained using $V_c = \sqrt{2}\sigma$ (for a spherical halo). The derived value of $\langle \sigma^2 \rangle^{1/2}$ depends on the selection of the sample of lens galaxies, which hampers a direct comparison with other studies.

It is more useful to compute the velocity dispersion of a galaxy with some fiducial luminosity, for which we take $L_B = 10^{10}h^{-2}L_{B\odot}$. To do so, we have to adopt a scaling relation between the velocity dispersion and the luminosity. We assume $\sigma \propto L_B^{0.3}$ (see §4). Under these assumptions we obtain a velocity dispersion $\sigma = 140 \pm 4$ km/s for a galaxy with $L_B = 10^{10}h^{-2}L_{B\odot}$. Hoekstra et al. (2003) measured $\sigma = 115_{-17}^{+15}$ km/s for a galaxy with a luminosity of $5.6 \times 10^{9}h^{-2}L_{B\odot}$ using a sample of galaxies with redshifts from CNOC2. Scaling our measurements to this luminosity implies a velocity dispersion of 118 ± 4 km/s, in excellent agreement with Hoekstra et al. (2003).

4. PROPERTIES OF DARK MATTER HALOS

The galaxy-mass cross-correlation function is the convolution of the galaxy distribution and the galaxy dark matter profiles. To examine the ensemble average properties of the dark matter halos properly, we need to deconvolve the galaxy-mass cross-correlation function (i.e., we need to account for the clustering of the lenses). This is done naturally in a maximum likelihood analysis, where a model for the mass distribution of individual galaxies is compared to the observations.

Fisher et al. (2002) and McKay et al. (2001) used a model with the velocity dispersion and “extent” of the halo as free parameters, and computed the resulting galaxy-mass correlation function for a range of model parameters and compared the results to the observed galaxy-mass correlation function. They obtained good constraints for the velocity dispersion, but were not able to constrain the extent of the dark matter halos.

An isolated lens induces a purely tangential distortion, but this is no longer the case for an ensemble of lenses. The galaxy-mass correlation function only uses the tangential component of the distortion, and ignores additional information contained in the other component. Hoekstra et al. (2003) compared their mass model to the observed polarisation field, making use of both components of the polarisation (also see Brainerd et al. 1996; Schneider & Rix 1997; Hudson et al. 1998). This greatly improved the constraints on the extent of the halo, and we will use the same method here.

In our analysis we make an important assumption: all clustered matter is associated with the lenses. If the matter in galaxy groups (or clusters) is associated with the halos of the group members (i.e., the halos are indistinguishable from the halos of isolated galaxies) our results should give a fair estimate of the extent of galaxy halos. However, if a significant fraction of the dark matter is distributed in common halos, a simple interpretation of the

results becomes more difficult.

Hoekstra et al. (2003) examined how known groups in their observed fields affected the lensing results, and found that the masses and sizes might be overestimated by at most $\sim 10\%$. Guzik & Seljak (2002) found similar results from their analysis of the galaxy-galaxy lensing signal in the context of halo models. Their approach allows one to separate the contribution from groups to the lensing signal. As expected, Guzik & Seljak (2002) found that the effect depends on galaxy type: early type galaxies are found in high density regions, and are affected more. Alternatively, a comparison with numerical simulations which include a prescription for galaxy formation (e.g., Kauffmann et al. 1999a, 1999b; Guzik & Seljak 2001) can be used to quantify this effect.

Another complication is the fact that we cannot separate the lenses in different morphology classes with the current data. Early and late type galaxies of a given luminosity have different masses, etc. (e.g., Guzik & Seljak 2002). Hence, it is important to keep in mind that the results presented here are ensemble averages over all galaxy types. This is where the SDSS can play an important role, although we can significantly improve the RCS results with upcoming multi-color data.

The scatter in the polarisations is approximately constant with apparent magnitude and can be approximated by a Gaussian distribution. In this case the log-likelihood follows a χ^2 distribution with the number of degrees of freedom equal to the number of free model parameters, and the determination of confidence intervals is straightforward. The log-likelihood is given by the sum over the two components of the polarisation e_i of all the source galaxies

$$\log \mathcal{L} = - \sum_{i,j} \left(\frac{e_{i,j} - P_j^\gamma g_{i,j}^{\text{model}}}{\sigma_{e_j}} \right)^2, \quad (1)$$

where $g_{i,j}$ are the model distortions, P_j^γ is the shear polarisability, $e_{i,j}$ are the observed image polarisations for the j th galaxy, and σ_{e_j} is the uncertainty in the measurement of the polarisation of the j th galaxy. In order to minimize the contribution of the baryonic (stellar) component of the galaxies we compare our model to the observations at radii larger than 10 arcseconds (which corresponds to $\sim 30h^{-1}$ kpc at the redshift of the lenses), where the dark matter halo should dominate the lensing signal.

In our maximum likelihood analysis we ignore the contribution from lenses outside the field of view (e.g., Hudson et al. 1998). For small fields of view this tends to slightly lower the resulting halo masses and sizes. The area covered by our observations is much larger than the HDF North studied by Hudson et al. (1998), and the effect on our estimates is negligible.

To infer the best estimates for the model parameters, one formally has to perform a maximum likelihood analysis in which the redshift of each individual galaxy is a free parameter, which has to be chosen such that it maximizes the likelihood. This approach is computationally not feasible, and instead we create mock redshift catalogs, using the observed redshift distributions from the CNOC2 survey (Hoekstra et al. 2003), which allows us to find estimates for the model parameters.

The redshifts of the galaxies in the mock catalogs are drawn randomly for the CNOC2 survey based on their apparent R_C magnitude. We take the incompleteness of the survey into account when the redshifts are drawn from the survey. In effect we use the apparent R_C magnitude as a crude redshift indicator. Although this procedure does not provide the formal maximum likelihood parameter estimation, it does yield an unbiased estimate of the parameters. The procedure is repeated 10 times and enables us to properly account for the uncertainty introduced by the lack of precise redshifts for the lenses.

Future multi-color catalogs will improve the results presented here significantly. Nevertheless, the large number of lenses and sources in the RCS data allows us to derive useful constraints on the properties of the dark matter halos surrounding the lenses.

In §4.1 we consider the Truncated Isothermal Sphere (TIS; e.g., Brainerd et al. 1996; Schneider & Rix 1997; Hoekstra et al. 2003), which has been used previously in galaxy-galaxy lensing analyses. In §4.2 we compare the data to the popular NFW profile (Navarro et al. 1995, 1996, 1997).

4.1. Truncated Isothermal Sphere Model

A simple model is the truncated isothermal sphere proposed by Brainerd et al. (1996). Its density profile is given by

$$\rho(r) = \frac{\sigma^2 s^2}{2\pi G r^2 (r^2 + s^2)}, \quad (2)$$

where σ is the line-of-sight velocity dispersion, and s is a truncation scale, i.e. the radius where the profile steepens. On small scales ($r \ll s$) the model behaves as an Singular Isothermal Sphere (SIS) model, whereas for $r \gg s$ the density decreases $\propto r^{-4}$. The mass contained within a sphere of radius r is given by

$$M(r) = \frac{2\sigma^2 s}{G} \arctan(r/s), \quad (3)$$

which results in a finite total mass of

$$M_{\text{tot}} = \frac{\pi\sigma^2}{G} s = 7.3 \times 10^{12} \left(\frac{\sigma}{100 \text{ km/s}} \right)^2 \left(\frac{s}{1 \text{ Mpc}} \right). \quad (4)$$

The projected surface density for this model is given by

$$\Sigma(r) = \frac{\sigma^2}{2Gr} \left(1 - \frac{r}{\sqrt{r^2 + s^2}} \right). \quad (5)$$

The corresponding expressions for the shear can be found in Brainerd et al. (1996) and Schneider & Rix (1997).

We use this model to compute the model shear field and compare it to the data. The lenses, however, span a range in masses and we need to account for that using scaling relations, which allow us to relate the halo properties of the lenses to those of a fiducial galaxy. For the fiducial galaxy we take a luminosity of $L_B = 10^{10} h^{-2} L_{B\odot}$, and we assume that

$$\sigma \propto L_B^{\beta/2}, \text{ and } s \propto L_B^\eta. \quad (6)$$

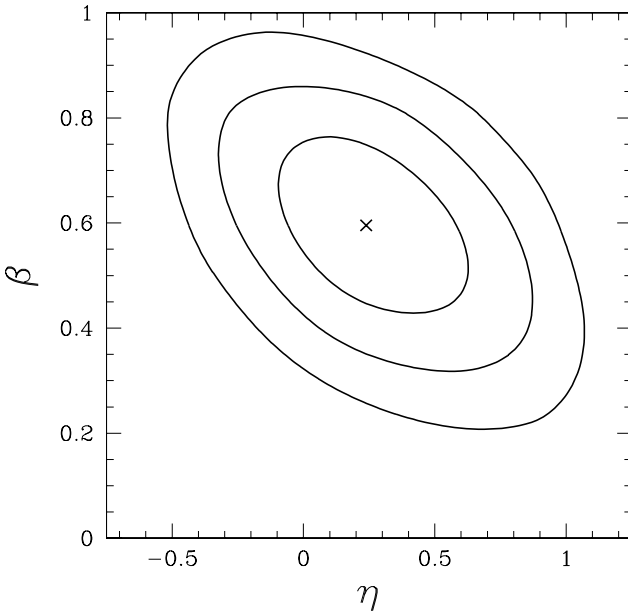


FIG. 4.— Joint constraints on β and η from the maximum likelihood analysis using a truncated isothermal sphere model. The cross indicates the best estimates for β and η . The contours indicate the 68.3%, 95.4%, and the 99.7% confidence on two parameters jointly. The inferred value for β is in excellent agreement with the slope of the observed B -band Tully-Fisher relation.

Consequently, the total mass of the galaxy scales with luminosity as

$$M_{\text{tot}} \propto L^\alpha, \text{ with } \alpha \equiv \beta + \eta. \quad (7)$$

Dynamical studies provide evidence of a power law scaling relation between the velocity dispersion and the luminosity (e.g., Tully-Fisher relation for spiral galaxies and Faber-Jackson relation for early type galaxies), with values for $\beta = 0.5 - 0.6$ in the B band. Little is known, however, about the relation of the extent of dark matter halos with other (observable) parameters.

We first examine how well the RCS data can constrain the parameters in the adopted scaling relations. We marginalise over the values for σ and s to obtain joint constraints on β and η . The results are presented in Figure 4. Even with the crude estimates for the luminosities of the lenses that are currently available, we can place useful constraints on the scaling relations for the velocity dispersion and the truncation parameter. Improved redshift information is expected to reduce the uncertainties by a factor ~ 2 .

We find a value of $\beta = 0.60 \pm 0.11$ (68% confidence, marginalized over all model parameters), which implies a slope of 0.30 ± 0.06 for the B -band Tully-Fisher relation. This result is in excellent agreement with the observed slope of the B -band Tully-Fisher relation (e.g., Verheijen 2001). For the scaling relation between the luminosity and the truncation parameter, we obtain $\eta = 0.24^{+0.26}_{-0.22}$. Hence the extent of the halo depends relatively weakly on the luminosity. Finally, we can combine these parameters to find the scaling relation between the total mass of the halo and the luminosity. Our measurements yield $\alpha = \beta + \eta = 0.84^{+0.28}_{-0.25}$.

Having constrained these scaling relations, we now turn to the properties of our fiducial galaxy. Figure 5 shows the joint constraints on the velocity dispersion σ and truncation parameter s for a fiducial galaxy with $L_B = 10^{10} h^{-2} L_{B\odot}$. Conveniently, for this particular luminosity, the inferred values of the velocity dispersion and truncation parameter depend only marginally on the adopted scaling relations.

For the velocity dispersion we obtain a value of $\sigma = 137 \pm 5$ km/s (68% confidence, marginalizing over all other model parameters). Hoekstra et al. (2003) find a velocity dispersion of $\sigma = 110 \pm 12$ for a galaxy with a luminosity of $5.6 \times 10^9 h^{-2} L_{B\odot}$. For a galaxy with that luminosity, our scaling relations imply a velocity dispersion of 114 ± 4 km/s, in excellent agreement with Hoekstra et al. (2003). McKay et al. (2001) who found a best fit value of $\sigma = 113^{+17}_{-13}$ km/s (95% confidence) for a galaxy with $L_{g'} \sim 9 \times 10^9 h^{-2} L_{g'\odot}$. Our results correspond to a velocity dispersion of $\sigma = 128 \pm 5$ km/s for a galaxy of that luminosity, in good agreement with the SDSS result.

We derive tight constraints on the truncation parameter, i.e. the extent of dark matter halos. We find a value of $s = 185^{+30}_{-28} h^{-1}$ kpc (68% confidence), and a total mass $M_{\text{tot}} = (2.5 \pm 0.3) \times 10^{12} h^{-1} M_\odot$.

The results presented in Hoekstra et al. (2003) imply a value of $s = 293^{+127}_{-86} h^{-1}$ kpc (68% confidence) for their fiducial galaxy. For a galaxy with a luminosity of $5.6 \times 10^9 h^{-2} L_{B\odot}$, we obtain $s = 157^{+38}_{-30} h^{-1}$ kpc (the error includes the uncertainty in the value of η), marginally consistent with Hoekstra et al. (2003).

4.2. NFW model

Numerical simulations of collisionless cold dark matter (CDM) reproduce the observed structure in the universe remarkably well. Furthermore these simulations suggest that CDM gives rise to a specific density profile, which fits the radial mass distribution for halos with a wide range in mass (e.g., Dubinski & Carlberg 1991; Navarro et al. 1995, 1996, 1997). The NFW density profile is characterized by 2 parameters, a density contrast δ_c and a scale r_s

$$\rho(r) = \frac{\delta_c \rho_c}{(r/r_s)(1+r/r_s)^2}, \quad (8)$$

where ρ_c is the critical surface density at the redshift of the halo. The “virial” radius r_{200} is defined as the radius where the mass density of the halo is equal to $200\rho_c$, and the corresponding mass M_{200} inside this radius is given by

$$M_{200} = \frac{800\pi}{3} \rho_c r_{200}^3. \quad (9)$$

The concentration parameter is defined as $c = r_{200}/r_s$, which yields an expression for the overdensity of the halo δ_c in terms of c

$$\delta_c = \frac{200}{3} \frac{c^3}{\ln(1+c) - c/(1+c)}. \quad (10)$$

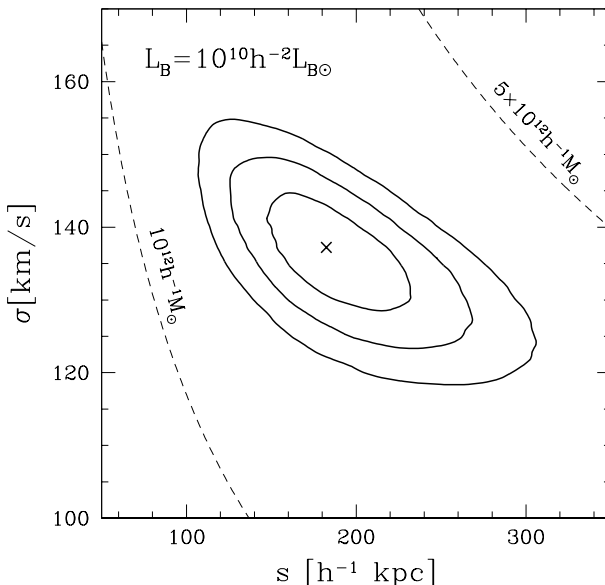


FIG. 5.— Joint constraints on the velocity dispersion σ and truncation parameter s for a fiducial galaxy with $L_B = 10^{10} h^{-2} L_{B\odot}$. The contours indicate the 68.3%, 95.4%, and the 99.7% confidence on two parameters jointly. The cross indicates the best fit value. The dashed lines indicate models with masses $M_{\text{tot}} = 10 \times 10^{12} h^{-1} M_\odot$ and $M_{200} = 5 \times 10^{12} h^{-1} M_\odot$.

It is important to note that the density profile on small scales remains controversial as other groups find different results (e.g., Moore et al. 1999; Ghigna et al. 2000). In addition, realistic simulations should include the effect of baryons, which complicate matters even further (see e.g., Mo, Mao & White 1998; Kochanek & White 2001). Unfortunately the current RCS data do not allow us to constrain the slope of the inner mass profile. However, future, deep lensing surveys, such as the CFHT Legacy Survey, will be well suited for such a study.

On the other hand, there is good agreement for the density profile on large scales, and a comparison of the profiles of real objects with the predictions provides an important test of the assumption that structures form through dissipationless collapse. The predicted profiles agree well with the observed mass distribution in clusters of galaxies (e.g., Hoekstra et al. 2002d), but the situation is less clear for galaxy mass halos. Rotation curves can provide some constraints, but typical values for r_s for galaxy mass halos are $10 - 20 h^{-1}$ kpc, comparable to the outermost point for which rotation curves have been measured.

Galaxies that are thought to be dark matter dominated, such as low surface brightness galaxies, potentially might be more suitable to test the CDM predictions. Studies of the rotation curves of low surface brightness galaxies suggest that, at least for a fraction of them, the observed rotation curves rise more slowly than the CDM predictions (e.g., de Blok, McGaugh & Rubin 2001; McGaugh, Barker & de Blok 2002). It is not clear, however, whether such studies provide a good test of CDM, because low surface brightness galaxies are peculiar (Zwaan & Briggs 2000), and their formation is not well understood. Hence, it is not obvious that their halos should be described by an

NFW profile. Recently Ricotti (2003) has suggested that the inner slope might depend on halo mass, with low mass systems having shallow cores, whereas massive galaxies are well described by the NFW profile.

In this section we compare the NFW profile to the observations, with δ_c and r_s as free parameters. The equations describing the shear for the NFW profile have been derived by Bartelmann (1996) and Wright & Brainerd (2000). We assume that the value of r_s is constant over the redshift range considered here, which is supported by the results of Bullock et al. (2001).

In the maximum likelihood analysis we derive joint constraints on δ_c and r_s for which we assume the following scaling relations

$$\delta_c \propto L_B^\beta, \text{ and } r_s \propto L_B^{\eta/2}, \quad (11)$$

As before, we first constrain the parameters of the scaling relations. We marginalise over the values for δ_c and r_s to obtain joint constraints on β and η . For this particular case it is more convenient to constrain $\beta + \eta$ and η , and the results are presented in Figure 6.

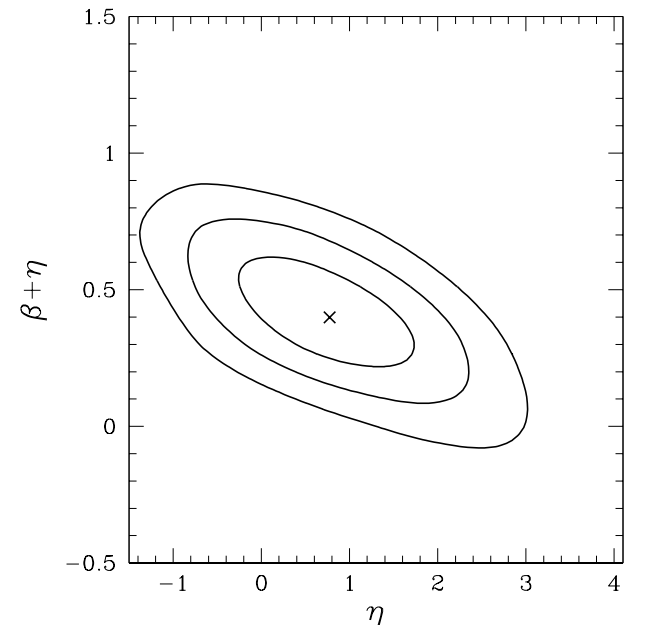


FIG. 6.— Joint constraints on $\beta + \eta$ and η from the maximum likelihood analysis using an NFW model. The cross indicates the best estimates for $\beta + \eta$ and η . The contours indicate the 68.3%, 95.4%, and the 99.7% confidence on two parameters jointly. The mass M_{200} scales approximately with luminosity $\propto L_B^{1.5(\beta+\eta)}$.

Figure 6 shows that the sum $\beta + \eta$ is fairly well constrained. We obtain a best fit value of $\beta + \eta = 0.40^{+0.14}_{-0.13}$ (68% confidence). For η we find $\eta = 0.77^{+0.63}_{-0.67}$. Our adopted scaling relations imply the mass M_{200} scales with luminosity as a power law with an approximate exponent $\alpha \approx 1.5(\beta + \eta)$. Our results are in fair agreement with this expectation and we find a best fit value of $\alpha = 0.70 \pm 0.33$ (68% confidence; confidence interval determined from a Monte Carlo simulation). This result is fairly similar to the one obtained from the TIS model in §4.1. Also the relation between the maximum rotation velocity V_{max} and the luminosity is well described by a power law, with an

exponent $0.20^{+0.13}_{-0.14}$ (68% confidence) in good agreement with the observed slope of the Tully-Fisher relation (e.g., Verheijen 2001).

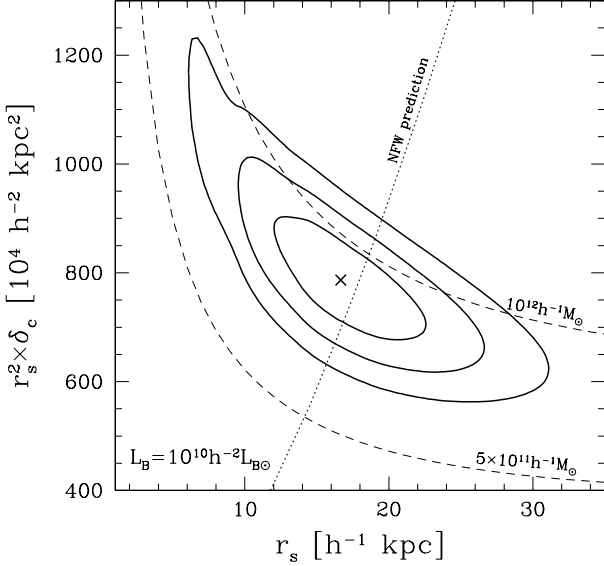


FIG. 7.— Joint constraints on $\delta_c r_s^2$ and scale radius r_s for a fiducial galaxy with $L_B = 10^{10} h^{-2} L_{B\odot}$, with an NFW profile. The contours indicate the 68.3%, 95.4%, and the 99.7% confidence on two parameters jointly. The cross indicates the best fit value. The dashed lines indicate models with masses $M_{200} = 5 \times 10^{11} h^{-1} M_\odot$ and $M_{200} = 10^{12} h^{-1} M_\odot$. The dotted line indicates the predictions from the numerical simulations, which are in excellent agreement with our results.

Figure 7 shows the joint constraints on $r_s^2 \delta_c$ (we chose this combination for computational convenience) and r_s for a galaxy with a luminosity of $L_B = 10^{10} h^{-2} L_{B\odot}$. The mass M_{200} is well constrained, and we derive a best fit value of $M_{200} = (8.8 \pm 0.7) \times 10^{11} h^{-1} M_\odot$ (68% confidence), and a corresponding value of $r_{200} = 138^{+3}_{-5} h^{-1}$ kpc. It is useful to compare this result with the mass from the TIS model. The TIS model yields $M_{\text{TIS}}(r_{200}) = (1.0 \pm 0.1) \times 10^{12} h^{-1} M_\odot$, which is slightly larger than the NFW value. As shown by Wright & Brainerd (2000), isothermal models give higher masses compared to NFW models. Hence, the results derived from both models are consistent.

From their galaxy-galaxy lensing analysis of the SDSS, Guzik & Seljak (2002) find $M_{200} = (9.3 \pm 1.6) \times 10^{11} h^{-1} M_\odot$ for a galaxy of $L_{g'} \sim 1.1 \times 10^{10} h^{-2} L_{g'\odot}$, in good agreement with our results. Guzik & Seljak (2002) also constrained the scaling relation between luminosity and M_{200} and find a slope $\alpha = 1.16 \pm 0.22$ in the g' -band, which is consistent with our value of 0.70 ± 0.33 .

Theoretical models predict that the galaxy mass-to-light ratio reaches minimum near L_* , where galaxy formation is most efficient (Benson et al. 2000). Consequently, the scaling relation between luminosity and mass depends on the lens sample, complicating the interpretation of our result. As noted by Guzik & Seljak (2002) most of the lensing signal in their SDSS sample comes from massive galax-

ies, much brighter than L_* , whereas the signal in the RCS sample is dominated by galaxies around L_* , which might explain the lower value of α found in this paper.

With multi-color data from the RCS and more data from the SDSS the statistical uncertainties are expected to decrease significantly over the coming few years. With such data it is feasible to constrain the scaling relation between mass and light as a function of mass, thus providing an important test of models of galaxy formation.

For the scale r_s we find $r_s = 16.7^{+3.7}_{-3.0} h^{-1}$ kpc (68% confidence), and the best fit density contrast is $\delta_c = 2.8^{+1.6}_{-0.9} \times 10^4$ (68% confidence; confidence interval from Monte Carlo simulation). The TIS model provides a slightly better fit to the data, but the difference is not significant, and consequently the data are not sufficient to distinguish between the NFW and TIS model.

In our maximum likelihood analysis we considered r_s and δ_c free parameters. Numerical simulations of CDM, however, show that the parameters in the NFW model are correlated, albeit with some scatter. As a result, the NFW model can be considered as a one-parameter model: given the cosmology, redshift, and one of the NFW parameters, the values for all other parameters can be computed using the routine **CHARDEN** made available by Julio Navarro¹. Hence, the simulations make a definite prediction for the value of $\delta_c r_s^2$ as a function of r_s . The dotted line in Figure 7 indicates this prediction. If the simulations provide a good description of dark matter halos, the dotted line should intersect our confidence region, which it does.

This result provides important support for the CDM paradigm, as it predicts the correct “size” of dark matter halos. It is important to note that this analysis is a direct test of CDM (albeit not conclusive), because the weak lensing results are inferred from the gravitational potential at large distances from the galaxy center, where dark matter dominates. Most other attempts to test CDM are confined to the inner regions, where baryons are, or might be, important.

4.3. Mass-to-light ratio

The observed average mass-to-light ratio of clusters has been used extensively to estimate the mean mass-to-light ratio of the universe. Multiplying the derived mass-to-light ratio with the observed luminosity density yields an estimate of the matter density. An important assumption in this method is that the cluster mass-to-light ratios can provide an estimate of the “universal” mass-to-light ratio.

The galaxy properties of rich cluster are different from the field, and a correction is needed to relate the cluster mass-to-light ratio to an estimate of Ω_m . Doing so, Carlberg et al. (1997) derived a value of $\Omega_m = 0.19 \pm 0.06$, based on a sample of 16 clusters. Galaxy groups are more representative of the field and a smaller correction for the difference in galaxy population is needed. Hoekstra et al (2001a) obtained a value of $\Omega_m = 0.19 \pm 0.1$ from a weak lensing analysis of 50 groups. Bahcall & Comerford (2002) found $\Omega_m = 0.17 \pm 0.05$ from a combination of clusters and groups taken from the literature.

Consequently, the mean mass-to-light ratio of all galaxies is a quantity of great interest, because it can be used to estimate the matter density “directly” (i.e., without ad-

¹ The routine **CHARDEN** can be obtained from <http://pinot.phys.uvic.ca/~jfn/charden>

ditional corrections for differences in properties). In this section we examine how our results can be used to measure the average mass-to-light ratio of the universe.

Having constrained the scaling relations and the mass of a $L_B = 10^{10}h^{-2}L_{B\odot}$ galaxy, we can convert the luminosity function into a galaxy mass function, and derive the corresponding mass density. We use the luminosity function of field galaxies determined from the CNOC2 survey (Lin et al. 1999). This luminosity function is well matched to our sample of lenses, because of the similar selection in apparent magnitude. The corresponding luminosity density at the mean lens redshift is $j = (3.0 \pm 0.6) \times 10^8 h L_{B\odot} \text{Mpc}^{-3}$ (Lin et al., 1999).

The first complication is the definition of the mass of a galaxy. Although the total mass of the TIS model is finite, it is actually not sensible to use M_{tot} , because matter at large radii is not bound to the galaxy. We use the virial mass instead. The NFW model and the TIS model give slightly different values: for a $L_B = 10^{10}h^{-2}L_{B\odot}$ galaxy, the TIS model yields a mass-to-light ratio of $M_{200}/L_B = 100 \pm 10 M_\odot/L_{B\odot}$, whereas the NFW value is $M_{200}/L_B = 88 \pm 7 M_\odot/L_{B\odot}$.

To obtain the mean mass-to-light ratio, we need to integrate over the luminosity function and the mass function derived using the scaling relations. The result depends only weakly on the lower limit for the mass. We use a mass limit of $10^{10}h^{-1}M_\odot$, which yields a mean mass-to-light ratio of $\langle M_{200}/L_B \rangle = 98_{-14}^{+41} M_\odot/L_{B\odot}$ for the NFW model (68% confidence; the confidence limits were derived from a Monte Carlo simulation of the statistical errors). The TIS model gives $\langle M_{200}/L_B \rangle = 100_{-11}^{+12} M_\odot/L_{B\odot}$, similar to the NFW model. The error bars are smaller, because the TIS scaling relation results in a smaller variation of the mass-to-light ratio as a function of luminosity.

These mass-to-light ratios imply a value of the matter density in galaxies (with respect to the critical density) $\Omega_m^{\text{gal}} = 0.11_{-0.02}^{+0.05}$. To obtain the total matter density, we need to account for the amount of matter that is not associated with galaxies. To this end, we use the high resolution numerical simulations of the local universe, which were done by the GIF collaboration². The simulations are described in Mathis et al. (2002).

We use the halo catalogs of the Λ CDM and τ CDM simulation to estimate which fraction of the mass is contained within halos with masses larger than $10^{10}h^{-1}M_\odot$. To derive this fraction f , we sum the virial masses of the halos, and divide by the total mass of the simulation volume. For the Λ CDM simulation we find a value of $f = 0.38 \pm 0.05$. The error bar has been estimated from the variation in f for four different subsets of the simulation. For the τ CDM model we find a similar value of $f = 0.33 \pm 0.03$. Hence, a significant number of particles are not associated with halos above our mass limit.

We use the results from the Λ CDM model to estimate Ω_m , because this model is more appropriate for our analysis (note that the value of f does not vary significantly with cosmology). Doing so, we obtain $\Omega_m = 0.30_{-0.08}^{+0.12}$ (68% confidence), in excellent agreement with recent measurements using other techniques (e.g., Spergel et al. 2002, Contaldi, Hoekstra & Lewis 2003).

To correct for the fraction of matter not associated with

galaxies, we assumed that all halos in the simulations contain galaxies. If there are large numbers of dark halos, the correction should have been larger. This might be relevant for our mass limit of $10^{10}h^{-1}M_\odot$. We verified whether a larger mass limit would change our result and find that our estimate for Ω_m is robust: e.g., confining the analysis to masses larger than $10^{11}h^{-1}M_\odot$ yields a slightly lower mean mass-to-light ratio and f , but leaves the resulting value for Ω_m unchanged.

5. SHAPES OF HALOS

The average shape of dark matter halos can provide important information about the nature of dark matter. Numerical simulations of cold dark matter yield triaxial halos, with a typical ellipticity of ~ 0.3 (e.g., Dubinski & Carlberg 1991). Hence, in the context of collisionless cold dark matter, the theoretical evidence for flattened halos is quite strong. If the dark matter is interacting, it tends to produce halos that are more spherical (compared to cold dark matter). This difference is more pronounced in the central parts of the halo, where the density is high. On the large scales probed by weak lensing, the different types of dark matter (for reasonable interaction cross-sections) produces halos with similar shapes.

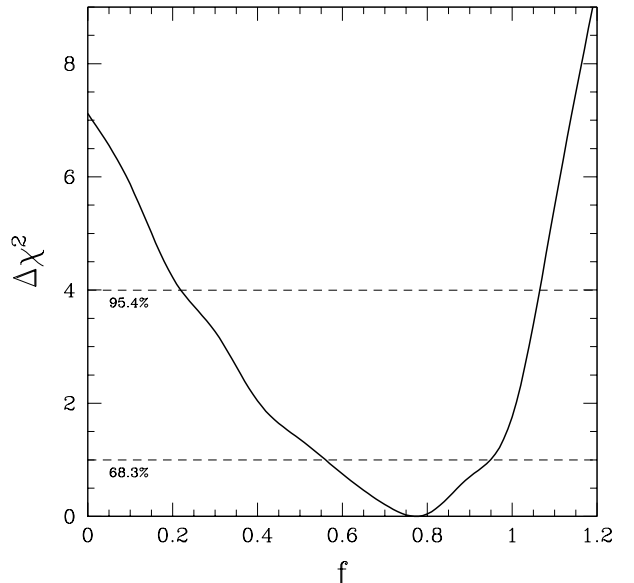


FIG. 8.— $\Delta\chi^2$ as a function of f . We have assumed that the ellipticity of the halos is related to the observed ellipticity of the lens as $e_{\text{halo}} = fe_{\text{lens}}$. We have indicated the 68.3% and 95.4% confidence intervals. We find a best fit value of $f = 0.77_{-0.21}^{+0.18}$ (68% confidence). Round halos ($f = 0$) are excluded with 99.5% confidence.

Nevertheless, a measurement of the average shape of dark matter halos is important, because the observational evidence is still limited. Dynamical measurements are limited by the lack of visible tracers, and therefore only probe the vertical potential on scales ≤ 15 kpc. Although the spread in inferred values for the axis ratio c/a (where c/a is the ratio of the shortest to longest principle axis of the halo) is large, the results suggest an average value of

² The simulation products can be obtained from <http://www.mpa-garching.mpg.de/NumCos/CR>

$c/a = 0.5 \pm 0.2$ (Sackett 1999).

Weak gravitational lensing is potentially the most powerful way to derive constraints on the shapes of dark matter halos. The amount of data required for such a measurement, however, is large (e.g., Brainerd & Wright 2000; Natarajan & Refregier 2000): the galaxy-galaxy lensing signal is small, and now one needs to measure an even smaller azimuthal variation. We also have to assume that the galaxy and its halo are aligned. An imperfect alignment between light and halo will reduce the amplitude of the azimuthal variation detectable in the weak lensing analysis. Hence, weak lensing formally provides a lower limit to the average halo ellipticity.

Brainerd & Wright (2000) and Natarajan & Refregier (2000) proposed to study the azimuthal variation in the tangential shear around the lenses. On very small scales, the lensing signal is dominated by the lens, but on larger scales, the clustering of the lenses will lower the signal one tries to measure (the two point function is axisymmetric). We therefore use the maximum likelihood approach used in the previous section.

To maximize the signal-to-noise ratio of the measurement one has to assign proper weights to the lenses: edge-on galaxies have maximal weight, whereas the lensing signal around face-on galaxies contains no information about the shape of the halo. We adopt a simple approach, and assume that the (projected) ellipticity of the dark matter halo is proportional to the shape of the galaxy: $e_{\text{halo}} = f e_{\text{lens}}$.

The measurement of the azimuthally averaged tangential shear around galaxies is robust against residual systematics (e.g., imperfect correction for PSF anisotropy): contributions from a constant or gradient residual shear cancel. This is no longer the case for the quadrupole signal, and imperfect correction for the PSF anisotropy can mimick the signal from a flattened halo.

If the lens galaxy is oriented randomly with respect to the residual shear, the average over many lenses will cancel the contribution from systematics. In real data, however, the uncorrected shapes of the lenses are aligned with the systematic signal. Hence, an imperfect correction can give rise to a small quadrupole signal, although we note that the lenses used in our analysis are large compared to the PSF. We estimate the amplitude of this effect in Appendix A, and show that it is negligible for the measurements presented here. We also examined the robustness of our results by splitting the data into two samples and comparing the results.

We use an elliptical TIS model to compute the model shear field, and compare this to the data. Figure 8 shows the resulting $\Delta\chi^2$ as a function of f . We find a best fit value of $f = 0.77^{+0.18}_{-0.21}$ (68% confidence). This suggests that, on average, the dark matter distribution is rounder than the light distribution. As discussed above, our analysis formally provides only a lower limit on the halo ellipticity, and the true ellipticity might be higher if some of the halos are misaligned with the light. Nevertheless, the fact that we detect a significant flattening implies that the halos are well aligned with the light distribution. Also note that the lensing signal is caused by a range of different galaxy types, for which our simple relation between the halo ellipticity and light distribution might not be valid.

Consequently the interpretation of the results is difficult, although a simple interpretation actually yields sensible results. For instance, the average ellipticity of the lens galaxies is $\langle e_{\text{lens}} \rangle = 0.261$. Hence, the measured value of f implies an average projected halo ellipticity of $\langle e_{\text{halo}} \rangle = 0.20^{+0.04}_{-0.05}$ (68% confidence), which corresponds to an projected axis ratio of $c/a = 0.66^{+0.07}_{-0.06}$ (68% confidence). Although the weak lensing yields a projected axis ratio, the result is in fair agreement with the results from numerical simulations.

A robust outcome of our analysis is that spherical halos ($f = 0$) are excluded with 99.5% confidence. As we demonstrate below, this poses serious problems for alternative theories of gravity, which attempt to explain the observations without dark matter.

5.1. Implications for alternative theories of gravity

In this section we examine the implications of our measurement of the anisotropy in the lensing signal around galaxies for theories of gravity without dark matter. We focus on one particular approach: Modified Newtonian Dynamics (MOND; Milgrom 1983; Sanders 1986; Sanders & McGaugh 2002), which has been shown to describe rotation curves rather well (e.g., Begeman et al. 1991; Sanders & Verheijen 1998).

In principle weak lensing can be used as a powerful test of MOND, but unfortunately no relativistic description of MOND has been found. Consequently one cannot compute the lensing signal in this theory. However, even in the absence of an appropriate description of lensing, we can use the observed anisotropy in the lensing signal around galaxies to test MOND.

In any reasonable alternative theory of gravity, the anisotropy in the lensing signal of an *isolated* galaxy is caused by the distribution of light and gas in that galaxy. Hence, on small scales one expects an anisotropic signal, but at large radii (where there are no stars and gas) the anisotropy in the lensing signal decreases $\propto r^{-2}$. As a result, these theories predict an almost isotropic weak lensing signal on the scales probed by our analysis, which is not observed.

Galaxies, however, are not isolated and the external field effect (Milgrom 1986) might complicate the interpretation of our measurements. In MOND, if a galaxy is embedded in an external field, this field dominates the dynamics if its acceleration is larger than the acceleration of the galaxy. As a result, the effective gravitational field is non-spherical, even if the potential of the galaxy is isotropic (as is the case for an isolated galaxy).

This effect is important if galaxies would be aligned with this external field. We know, however, that the intrinsic alignments of galaxies are small (e.g., Lee & Pen 2001, 2002) and for the measurements presented here, it is safe to assume that the lenses have random orientation with respect to any external field. Consequently, the observed anisotropy in the lensing signal cannot be caused by the external field effect.

Hence, our findings provide strong support for the existence of dark matter, because alternative theories of gravity predict an almost isotropic lensing signal. Better constraints can be derived from future weak lensing surveys, which will allow us to study the anisotropy a function of

projected distance from the galaxy.

6. CONCLUSIONS

We have analysed the weak lensing signal caused by a sample of lenses with $19.5 < R_C < 21$ using 45.5 deg^2 of R_C band imaging data from the Red-Sequence Cluster Survey (RCS). We have studied the average mass profile around the lenses using a maximum likelihood analysis. To this end, we considered two models for the halo mass profile: a truncated isothermal sphere and an NFW profile. For both models we constrain the power law scaling relations between the B -band luminosity and the velocity dispersion (or rotation velocity) and the size of the halo.

The results for the velocity dispersion are in excellent agreement with the observed luminosity-line-width relations. The TIS model yields a best fit velocity dispersion of $\sigma = 137 \pm 5 \text{ km/s}$ and a truncation radius $s = 185^{+30}_{-28} h^{-1} \text{ kpc}$ for a galaxy with a fiducial luminosity of $L_B = 10^{10} h^{-2} \text{ L}_\odot$. Alternatively, the best fit NFW model yields a mass $M_{200} = (8.8 \pm 0.7) \times 10^{11} h^{-1} M_\odot$ and a scale radius $r_s = 16.7^{+3.7}_{-3.0} h^{-1} \text{ kpc}$. This value for the scale radius is in excellent agreement with predictions from numerical simulations for a halo of this mass. Having constrained the virial mass and scaling relations, we

can convert the observed luminosity function into a mass function, and estimate the matter density of the universe. Based on numerical simulations, we find that only $\sim 37\%$ of the matter is contained within the virial radius of halos. After correction for this effect, we obtain $\Omega_m = 0.30^{+0.13}_{-0.08}$, in excellent agreement with other recent measurements.

We also present the first detection of the flattening of galaxy dark matter halos from weak lensing. We use a simple model in which the ellipticity of the halo is f times the observed ellipticity of the lens. We find a best fit value of $f = 0.77^{+0.18}_{-0.21}$ (68% confidence), suggesting that the dark matter halos are somewhat rounder than the light distribution. The fact that we detect a significant flattening implies that the halos are aligned with the light distribution. Given the average ellipticity of the lenses, this implies a halo ellipticity of $\langle e_{\text{halo}} \rangle = 0.20^{+0.04}_{-0.05}$ (68% confidence), in fair agreement with results from numerical simulations of CDM. This result provides strong support for the existence of dark matter, as an isotropic lensing signal is excluded with 99.5% confidence.

The RCS project is partially supported by grants from the Natural Science and Engineering Science Council of Canada and the University of Toronto to HKCY.

REFERENCES

Bahcall, N.A., & Comerford, J.M. 2002, ApJ, 565, L5

Bartelmann, M. 1996, A&A, 313, 697

Begeman, K.G., Broeils, A.H., & Sanders, R.H. 1991, MNRAS, 249, 523

Benson, A.J., Cole, S., Frenk, C.S., Baugh, C.M., & Lacey, C.G. 2000, MNRAS, 311, 793

Bernstein, G.M. & Norberg, P. 2002, AJ, 124, 733

Brainerd, T.G., Blandford, R.D., & Smail, I. 1996, ApJ, 466, 623

Brainerd, T.G. & Wright, C.O. 2000, astro-ph/0006281

Bullock, J.S. et al. 2001, MNRAS, 321, 559

Carlberg, R.G., Yee, H.C., & Ellingson 1997, ApJ, 478, 462

Carlberg, R.G., Yee, H. K. C., Morris, S. L., Lin, H., Hall, P. B., Patton, D. R., Sawicki, M., & Shepherd, C. W. 2001, ApJ, 552, 427

Cohen, J.G. et al. 2000, ApJ, 538, 29

Contaldi, C.R., Hoekstra, H., & Lewis, A. 2003, PRL, 90, 221303

de Blok, W.J.G., McGaugh, S.S. & Rubin, V.C. 2001, AJ, 122, 2396

Dell'Antonio, I.P., & Tyson, J.A. 1996, ApJ, 473, L17

Dubinski, J. & Carlberg, R.G. 1991, ApJ, 378, 496

Fischer, P., et al. 2000, AJ, 120, 1198

Fernández-Soto, A., Lanzetta, K.M., & Yahil, A. 1999, ApJ, 513, 34

Ghigna, S., Moore, B., Governato, F., Lake, G., Quinn, T., Stadel, J. 2000, ApJ, 544, 616

Griffiths, R.E., Casertano, S., Im, M., & Ratnatunga, K.U. 1996, MNRAS, 282, 1159

Gladders, M.D. & Yee, H.K.C. 2003, to be submitted to ApJS

Guzik, J., & Seljak, U. 2001, MNRAS, 321, 439

Guzik, J., & Seljak, U. 2002, MNRAS, 335, 311

Hoekstra, H., Franx, M., Kuijken, K., & Squires, G. 1998, ApJ, 504, 636

Hoekstra, H., et al. 2001a, ApJ, 548, L5

Hoekstra, H., Yee, H.K.C., & Gladders, M.D. 2001b, ApJ, 558, L11

Hoekstra, H., Yee, H.K.C., Gladders, M.D., Barrientos, L.F., Hall, P.B., & Infante, L. 2002a, ApJ, 572, 55

Hoekstra, H., Yee, H.K.C., & Gladders, M.D. 2002b, ApJ, 577, 595

Hoekstra, H., van Waerbeke, L., Gladders, M.D., Mellier, Y., & Yee, H.K.C. 2002c, ApJ, 577, 604

Hoekstra, H., Franx, M., Kuijken, K., & van Dokkum, P.G. 2002d, MNRAS, 333, 911

Hoekstra, H., Franx, M., Kuijken, K., Carlberg, R.G., & Yee, H.K.C. 2003, MNRAS, 340, 609

Hudson, M.J., Gwyn, S.D.J., Dahle, H., & Kaiser, N. 1998, ApJ, 503, 531

Kauffmann, G., Colberg, J.M., Diaferio, A., White, S.D.M. 1999a, MNRAS, 303, 188

Kauffmann, G., Colberg, J.M., Diaferio, A., White, S.D.M. 1999b, MNRAS, 307, 529

Keeton, C.R., Kochanek, C.S., & Falco, E.E. 1998, ApJ, 509, 561

Kochanek, C.S., & White, M. 2001, ApJ, 559, 531

Lee, J. & Pen, U.-L. 2001, ApJ, 555, 106

Lee, J. & Pen, U.-L. 2001, ApJ, 567, L111

Lin, H., Yee, H.K.C., Carlberg, R.G., Morris, S.L., Sawicki, M., Patton, D.R., Wirth, G., & Shepherd, C.W. 1999, ApJ, 518, 533

Mathis, H., Lemson, G., Springel, V., Kauffmann, G., White, S. D. M., Eldar, A., & Dekel, A. 2002, MNRAS, 333, 739

McGaugh, S.S., Barker, M.K. & de Blok, W.J.G. 2002, astro-ph/0210641

McKay, T.A., et al. 2001, ApJ, submitted, astro-ph/0108013

McKay, T.A., et al. 2002, ApJ, 571, L85

Milgrom, M. 1983, ApJ, 270, 365

Milgrom, M. 1986, ApJ, 302, 617

Mo, H.J., Mao, S., & White, S.D.M. 1998, MNRAS, 295, 319

Moore, B., Quinn, T., Governato, F., Stadel, J., & Lake, G. 1999, MNRAS, 310, 1147

Natarajan, P. & Refregier, A. 2000, ApJ, 538, L113

Navarro, J.F., Frenk, C.S., & White, S.D.M. 1995, MNRAS, 275, 56

Navarro, J.F., Frenk, C.S., & White, S.D.M. 1996, ApJ, 462, 563

Navarro, J.F., Frenk, C.S., & White, S.D.M. 1997, ApJ, 490, 493

Ricotti, M. 2003, MNRAS, submitted, astro-ph/0212146

Sackett, P. 1999 in *Galaxy Dynamics*, ASP Conf. Series 182, eds. D.R. Merritt, M. Valluri, & J.A. Sellwood

Sanders, R.H., & McGaugh, S.S. 2002, ARA&A, 40, 263

Sanders, R.H., & Verheijen, M.A.W. 1998, ApJ, 503, 97

Sanders, R.H. 1986, MNRAS, 223, 539

Schneider, P., & Rix, H.-W. 1997, ApJ, 474, 25

Seljak, U. 2002, MNRAS, 334, 797

Smith, D.R., Bernstein, G.M., Fischer, P., & Jarvis, M. 2001, ApJ, 551, 643

Spergel, D.N. et al. 2003, ApJ, submitted, astro-ph/0302209

Tyson, J.A., Valdes, F., Jarvis, J.F., & Mills, A.P., Jr. 1984ApJ, 281, L59

van Albada, T.S., & Sancisi, R. 1986, Phil. Trans. Roy. Soc., London, A320, 447

Verheijen, M.A.W. 2001, ApJ, 563, 694

Wilson, G., Kaiser, N., Luppino, G.A. 2001, ApJ, 555, 572

Wright, C.O. & Brainerd, T.G. 2000, ApJ, 534, 34

Yee, H.K.C., et al. 2000, ApJS, 129, 475

Yee, H.K.C., & Gladders, M.D. 2001, in "AMiBA 2001: High-z Clusters, Missing Baryons, and CMB Polarization", ASP Conference Series, Eds. L.-W. Chen et al., astro-ph/0111431

Zaritsky, D., & White, S.D.M. 1994, ApJ, 435, 599

Zwaan, M.A. & Briggs, F.H. 2000, ApJ, 530, 61

APPENDIX

CONTRIBUTION OF SYSTEMATICS TO THE SHAPE MEASUREMENT OF DARK HALOS

In this appendix we examine how residual systematics affect the measurement of the flattening of dark matter halos. A schematic overview of the situation is presented in Figure A9. The thin lines indicate the direction of residual systematics. The residual shear has an amplitude $\hat{\gamma}$ and a position angle ϕ with respect to the major axis of the lens. The tangential shear γ_T^{obs} observed at a position (r, θ) is the sum of the lensing signal γ_T^{lens} and the contribution from systematics $\hat{\gamma}_T$. The latter is given by

$$\hat{\gamma}_T = -\hat{\gamma}[\cos(2\phi) \cos(2\theta) + \sin(2\phi) \sin(2\theta)] = -\hat{\gamma} \cos(2(\theta - \phi)). \quad (\text{A1})$$

Hence, the azimuthally averaged tangential shear is not affected by systematics as $\int d\theta \hat{\gamma}_T(\theta) = 0$, and the weak lensing mass estimate is very robust. For a flattened halo, the lensing signal γ_T^{lens} is given by

$$\gamma_T^{\text{lens}}(r, \theta) = [1 + \gamma_f \cos(2\theta)] \cdot \langle \gamma_T \rangle(r), \quad (\text{A2})$$

where $\langle \gamma_T \rangle$ is the azimuthally averaged tangential shear, and γ_f is a measure of the flattening of the halo. For positive values of γ_f , the halo is aligned with the lens.

We consider the worst case scenario, and demonstrate that even in this situation the results are robust. One way to estimate the flattening of the halo is to measure the shears γ_+ (at $\theta = 0$ and π), and γ_- (at $\theta = \pi/2$ and $3\pi/2$). The observed ratio $f = \gamma_-/\gamma_+$ is

$$f_{\text{obs}} = \frac{\gamma_- + \hat{\gamma} \cos(2\phi)}{\gamma_+ - \hat{\gamma} \cos(2\phi)}. \quad (\text{A3})$$

If ϕ is uncorrelated with the lens, the observed ratio, averaged over many lenses, is unaffected by systematics because $\langle \cos(2\phi) \rangle = 0$. However, in real data, the PSF anisotropy affects both the lens and the source galaxies. Although the lenses used in this paper are large compared to the PSF, any (small) residual in the correction will introduce a correlation in the position angle of the lens and the direction of the PSF anisotropy.

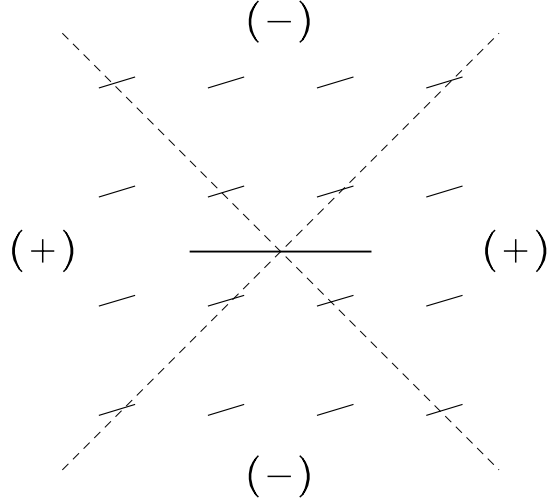


FIG. A9.— Schematic view of the lens galaxy and the residual systematic shear. If the dark halo is flattened and aligned with the lens (line in the center) then the tangential shear at a given radius is larger in the quadrants indicated by (+), and lower in (-). The small lines indicate the direction of the residual shear (e.g., caused by the imperfect correction for PSF anisotropy). The residual shear has an amplitude $\hat{\gamma}$ and has a direction with a position angle ϕ' with respect to the lens.

The effect is maximal for $\phi = 0$ (aligned with the major axis of the lens) or $\phi = \pi/2$ (perpendicular to major axis of the lens). The latter situation corresponds to an overcorrection of the PSF anisotropy, whereas the former occurs when the correction for PSF anisotropy is too small. For both (extreme) situations, only the observed value of γ_1 is affected by systematics (γ_2 is left unchanged). The observed value γ_1^{obs} for the lens can be written as $\gamma_1^{\text{obs}} = \gamma_1^{\text{true}} + \alpha \hat{\gamma}$, where α is a measure of the correlation between the position angle of the lens and the direction of the systematic shear of the background galaxies. In our case $\alpha \ll 1$, because the lenses are large compared to the PSF. For a lens with an observed $\gamma = \sqrt{\gamma_1^2 + \gamma_2^2}$, we find

$$\langle \cos(2\phi) \rangle = \frac{\alpha \hat{\gamma}}{2\gamma}. \quad (\text{A4})$$

The distribution of γ_1 and γ_2 can be approximated by a Gaussian with a dispersion σ (with a typical value of $\sigma = 0.2$). For the ensemble of lenses we then obtain

$$\langle \cos(2\phi) \rangle = \sqrt{\frac{\pi}{2}} \frac{\alpha \hat{\gamma}}{2\sigma}. \quad (\text{A5})$$

This introduces a relatively large signal because face-on lenses ($\gamma \approx 0$) align easily with the PSF anisotropy. Such lenses, however, contain no information about the shape of the halo. In our analysis we assign a weight $\propto \gamma$ to each lens. Hence in our case we are less sensitive to systematics as the correct estimate is given by

$$\langle \cos(2\phi) \rangle = \frac{\alpha \hat{\gamma}}{2}. \quad (\text{A6})$$

Hence, the observed ratio γ_-/γ_+ reduces to

$$f_{\text{obs}} = \frac{\gamma_- + \hat{\gamma}^2 \alpha/2}{\gamma_+ - \hat{\gamma}^2 \alpha/2} \quad (\text{A7})$$

We can now estimate how robust the measurement of the average halo shape is. We take a conservative estimate of $\alpha = 0.5$, and $\hat{\gamma} = 5 \times 10^{-3}$ (see Hoekstra et al. 2002a for a discussion of the residuals in our data). The average separation of stars in our data is ~ 1.5 and therefore the residual PSF anisotropy is likely to change direction on scales larger than the separation of the stars used to measure the anisotropy. The average tangential shear at 2 arcminutes is $\sim 5 \times 10^{-4}$. For a spherical halo ($\gamma_- = \gamma_+ = 5 \times 10^{-4}$) we would observe a ratio $f_{\text{obs}} = 1.025$. This corresponds to an ellipticity of 2.5% (with the halo oriented perpendicular to the lens), which is small.

In this very conservative estimate, we have assumed that for each lens, the residual PSF anisotropy is aligned with the lens (i.e., the PSF anisotropy was underestimated). There is, however, an equal probability of overestimating the PSF anisotropy. Hence, in reality the change in the ellipticity of the halo, caused by systematics is even smaller.